Boosting the Thermoelectric Performance of PbSe through Dynamic Doping and Hierarchical Phonon Scattering

Journal:	*Energy & Environmental Science*
Manuscript ID	EE-ART-02-2018-000418.R2
Article Type:	Paper
Date Submitted by the Author:	28-Apr-2018
Complete List of Authors:	You, Li; Shanghai University, School of Materials Science and Engineering Liu, Yefeng; Department of Electronic Information Materials, School of Materials Science and Engineering Li, Xin; Shanghai University, Materials Genome Institute Nan, Pengfei; Beijing Key Lab of Nanophotonics and Ultrafine Optoelectronic Systems Ge, Binghui; Chinese Academy of Sciences, Institute of Physics Jiang, Ying; Shanghai University, Materials Genome Institute Luo, Pengfei; Shanghai University, School of Materials Science and Engineering Pan, Shanshan; Shanghai University, School of Materials Science and Engineering Pei, Yanzhong; Tongji University, Materials Science Zhang, Wenqing; Southern University of Science and Technology, Department of Physics Snyder, G. Jeffrey; Northwestern University, Materials Science Yang, Jiong; Shanghai University, Materials Genome Institute Zhang, Jiye; Department of Electronic Information Materials, School of Materials Science and Engineering Luo, Jun; Shanghai University, School of Materials Science and Engineering

Broader context

Dynamic behaviors of atoms/ions in materials have attracted considerable attention because of the presence of singular and abundant physical properties. In this study, we demonstrate the temperature-driven diffusion of Cu ions in the PbSe lattice leads to a dynamic doping effect which optimizes the carrier concentration of the material in a wide temperature range. With the rising of temperature, more and more Cu ions enter into the PbSe lattice and provide extra charge carriers. In addition, the intercalation of Cu brings about not only hierarchical microstructures in the PbSe matrix but also on-site vibration of interstitial Cu ions at higher temperatures. Thus, the lattice thermal conductivity of the Cu intercalated PbSe is significantly reduced. Owing to the synergistic effects of dynamic doping and hierarchical phonon scattering on the thermoelectric transport properties, a peak zT value ~1.45 and device ZT about unity at 813 K are achieved in the n-type Cu-intercalated PbSe sample. Furthermore, all the samples exhibit prominent thermal stabilities, which is propitious to the long-term service performance of the related thermoelectric devices. This strategy proposed by us can be used as a general and effective method to improve the thermoelectric properties of all the lead chalcogenides based materials.

Journal Name

ARTICLE

Boosting the Thermoelectric Performance of PbSe through Dynamic Doping and Hierarchical Phonon Scattering†

Received 00th January 20xx,
Accepted 00th January 20xx

DOI: 10.1039/x0xx00000x

www.rsc.org/

Li You,‡[a] Yefeng Liu,‡[a] Xin Li,[b] Pengfei Nan,[c,d] Binghui Ge,[c] Ying Jiang,[b] Pengfei Luo,[a] Shanshan Pan,[a] Yanzhong Pei,[e] Wenqing Zhang,[f] G. Jeffrey Snyder,[g] Jiong Yang,*[b] Jiye Zhang,*[a] and Jun Luo*[a,b]

Here we find the peculiar behavior of Cu ions in the PbSe-Cu system increases its thermoelectric performance. For the electrical transport, a dynamic doping effect is achieved because more Cu ions enter into the PbSe lattice and provide extra charge carriers as the temperature increases, which guarantees optimized carrier concentration in a wide temperature range. For the thermal transport, the presence of Cu_2Se nanoprecipitates and dislocations at low temperature range as well as the vibration of Cu atoms around the interstitial sites of PbSe at high temperatures result in hierarchical phonon scattering and significantly reduced lattice thermal conductivity in the whole temperature range. As a result, a peak thermoelectric materials figure of merit zT up to 1.45 and thermoelectric device figure of merit ZT close to unity are attained in the sample with 0.375 at% Cu. Furthermore, enhanced thermoelectric properties are also realized in the Cu-intercalated PbS, implying that the temperature-driven dynamic behavior of Cu ions in a rigid lattice can serve as a general strategy to optimize the thermoelectric performance of IV-VI compounds.

Introduction

Exotic or even anomalous physical phenomena are often observed in material systems involving dynamic motion of atoms/ions, such as the recently discovered abnormal electrical and thermal transport properties in Cu_2Se with a liquid-like Cu sublattice,[1,2] or in VO_2 with a metal-insulator/structural transition.[3] Unfortunately, such exciting physical properties are usually accompanied by unstable crystal lattices, e.g., disordered sublattices or structural phase transitions, which seriously inhibits their future exploitation in advanced devices.[4-6] Therefore, it is desirable that similarly amazing electrical and thermal transport properties can also be achieved in a robust material with rigid lattice by simply intercalating an appropriate amount of mobile atoms/ions.

The performance of a thermoelectric material is jointly determined by its electrical and thermal transport properties.[7] The energy conversion efficiency of a thermoelectric material is regulated by its dimensionless thermoelectric figure of merit $zT = S^2\sigma T/\kappa_{tot}$, where S is the Seebeck coefficient, σ the electrical conductivity, T the absolute temperature, and κ_{tot} the total thermal conductivity. The total thermal conductivity κ_{tot} is composed of the electronic and lattice components κ_e and κ_L, respectively. Therefore, the thermoelectric material can be considered as an ideal system to utilize the aforementioned physical phenomena. Specifically, we can design a thermoelectric system comprising a host compound with rigid lattice and a small amount of precipitates as the reservoirs of mobile atoms/ions. As the temperature rises, the 'mobile atoms/ions' diffuse from the precipitates into the rigid lattice of the host compound, and then the dynamic motion of these atoms/ions can be activated at a certain temperature. This may bring about some physical effects beneficial to its electrical and thermal transport properties.

On the one hand, the temperature-driven diffusion of atoms/ions in a thermoelectric compound may lead to a dynamic doping effect. As a consensus of the thermoelectric community, carrier concentration optimization is a prior issue to maximize the thermoelectric performance of a given

[a] School of Materials Science and Engineering, Shanghai University, 99 Shangda Road, Shanghai 200444, China. E-mail: junluo@shu.edu.cn; jychang@shu.edu.cn
[b] Materials Genome Institute, Shanghai University, 99 Shangda Road, Shanghai 200444, China. E-mail: jiongy@t.shu.edu.cn
[c] Beijing National Laboratory for Condensed Matter Physics, Institute of Physics, Chinese Academy of Sciences, Beijing 100190, China.
[d] Beijing Key Lab of Nanophotonics and Ultrafine Optoelectronic Systems, School of Physics, Beijing Institute of Technology, Beijing 100081, China.
[e] School of Materials Science and Engineering, Tongji University, 4800 Caoan Road, Shanghai 201804, China.
[f] Shenzhen Key Laboratory of Thermoelectric Materials and Department of Physics, Southern University of Science and Technology, Shenzhen 518055, China.
[g] Department of Materials Science and Engineering, Northwestern University, Evanston, IL 60208, USA.

†Electronic Supplementary Information (ESI) available: Some calculation details; Phase identification, microstructure analysis, and in-situ heating STEM characterization (Fig. S1-S3); Discussions on the distinction between dynamic doping effect and bipolar effect (Fig. S4); Electronic density of states of Cu intercalated PbSe (Fig. S5); Lorenz number and electronic thermal conductivities (Fig. S6); Dislocation and platelet like nanoclusters in Cu intercalated samples (Fig. S7 and S8); Comparison of the electrical and thermal transport properties for PbSe with dynamic Cu doping and the conventional doping (Fig. S9-S11); Thermoelectric properties of $PbCu_xS$ (Fig. S12); Repeated measurement of thermoelectric properties and stability of the samples (Fig. S13-S16). See DOI: 10.1039/x0xx00000x

‡LY and YL contributed equally to this work.

material.[8-10] By assuming a single parabolic band conduction model, Ioffe has proposed that the optimal carrier concentration of a thermoelectric semiconductor usually increases with the rising of temperature.[11,12] However, in conventionally doped semiconductors, their carrier concentrations almost do not change with the temperatures. It is difficult to fully optimize the thermoelectric performance of a semiconductor over the whole working temperature range.[13] A possible approach to address this issue is functionally graded doping,[14,15] which is, unfortunately, not stable enough for practical applications.[13] The aforementioned dopant-rich precipitates in thermoelectric system might be good alternatives due to the dynamic doping effect.[9,16,17] They can be regarded as extrinsic dopant reservoirs embedded in the host matrix, which can continuously provide additional extrinsic charge carriers with the rising of temperature. Consequently, a graded carrier concentration matching well with the temperature might be attained for the thermoelectric material.[16]

On the other hand, the mobile atoms/ions in such a system may also result in anomalous thermal transport properties.[1] Reduced lattice thermal conductivity can be expected because of the phonon-phonon interactions from the loosely bonded atoms/ions, similar to the situation for the thermoelectric system with liquid-like ions， such as Cu_2Se and Cu_2S.[1,18] Even at low temperature range without the atomic diffusion, the nanoprecipitates should also contribute to κ_L reduction by the grain boundary scattering. The two-fold phonon scatterings take effects at different length scales, leading to the hierarchical scattering.[19] It is well known that a low κ_L is favored by the thermoelectric material since the total thermal conductivity is mostly determined by its lattice component.

In this work, we construct a phase separation system comprising PbSe host compound and Cu-rich precipitates at room temperature. As the temperature rises, the dynamic behaviors of Cu ions present in such a system. Firstly, Cu ions continuously diffuse from the Cu-rich precipitates into the rigid lattice of PbSe, rendering an optimized carrier concentration over a wide temperature range. Secondly, due to the hierarchical phonon scattering, i.e., the nanoprecipitates, dislocations and grain boundary scattering at low temperatures, and the low-lying optical phonons caused by the vibrations of Cu ions around the interstitial sites, lead to the ultralow lattice thermal conductivity of PbSe in the whole temperature range. Owing to the synergistic effects of dynamic doping and hierarchical phonon scattering on the thermoelectric transport properties, a peak zT value ~1.45 and device ZT about unity at 813 K are achieved in the n-type Cu-intercalated PbSe sample. Furthermore, all the samples exhibit prominent thermal stabilities, which is propitious to the long-term service performance of the related thermoelectric devices.

Results and discussion

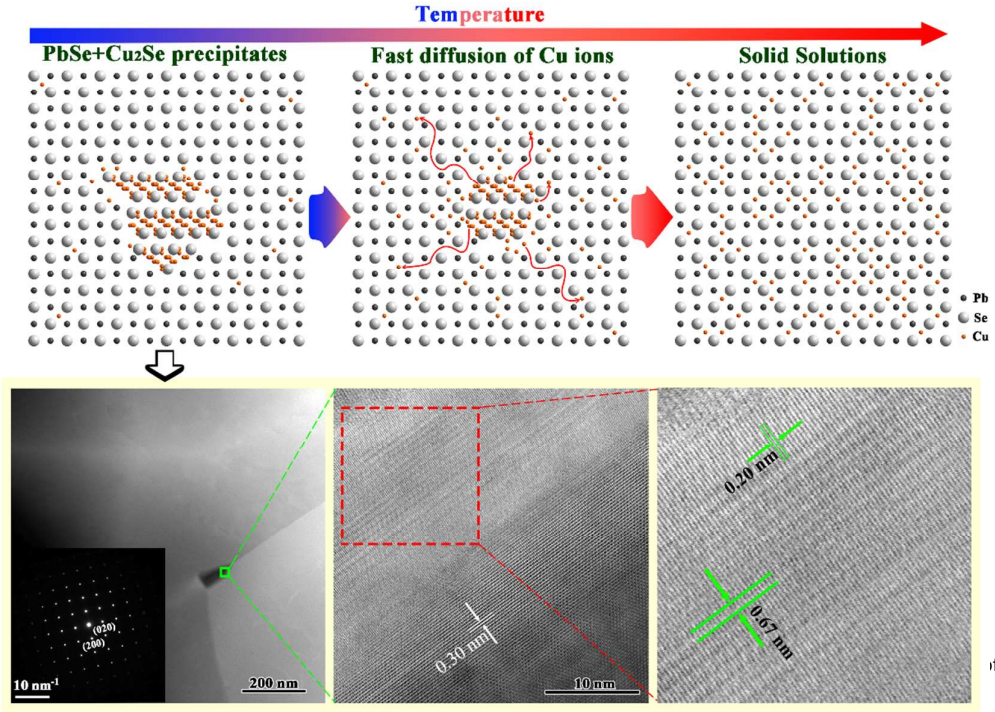

Fig. 1 Schematic illustration of the temperature dependent microstructure evolution for the phase-separated PbSe-Cu system (top panel) and the STEM images with different magnifications for the PbSe sample containing 0.75 at% Cu (bottom panel).

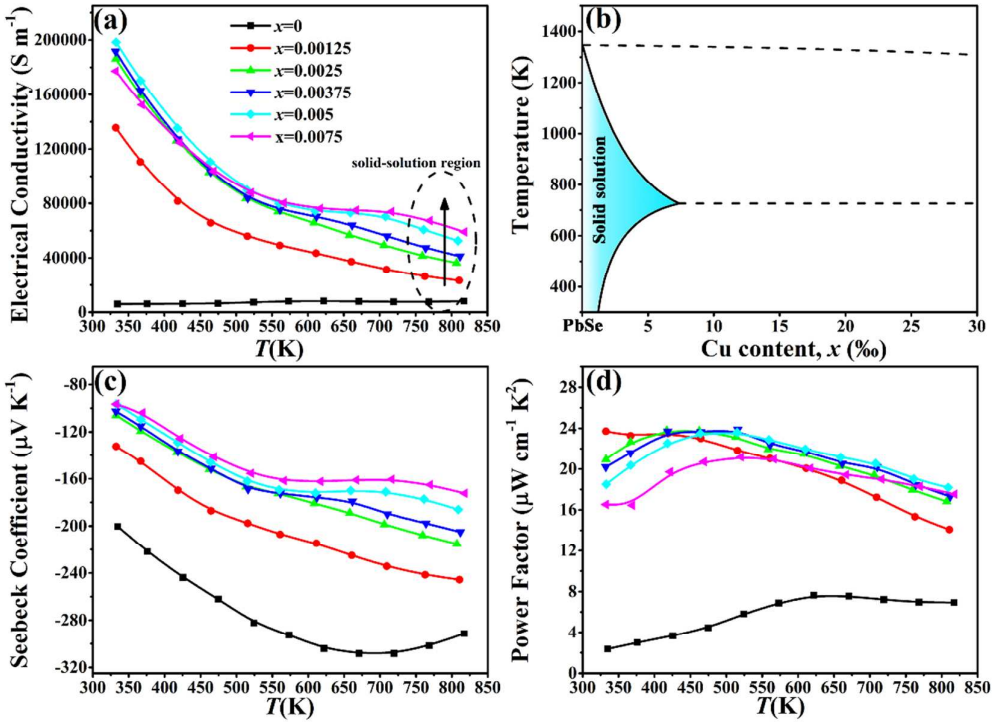

Fig. 2 Temperature dependence of (a) electrical conductivity, (c) Seebeck coefficient, and (d) power factor for the $PbCu_xSe$ samples. A schematic phase diagram describing the solid solubility of Cu in PbSe at different temperatures is shown in (b).

XRD analysis indicates that all the samples crystallize in the NaCl-type structure (see **Fig. S1** in the ESI†), but a very small amount of impurities may exist which is beyond the detection limit of the applied XRD technique. The temperature dependent microstructure evolution of the phase-separated PbSe-Cu system is schematically illustrated in the top panel of **Fig. 1**. For the PbSe-Cu system, the solubility of Cu in PbSe is very small at room temperature. Thus, Cu mainly exists in the precipitates as the Cu-rich selenide, and only extremely small amount of Cu ions reside in the interstitial sites of the PbSe lattice. It has been evidenced that the solute Cu atoms are located in the interstice of PbSe.[17] It is also to note that the Cu is an amphoteric dopant in the lead chalcogenide, depending on the specific composition of the lead chalcogenide.[20,21] In the Pb-riched condition, the Cu atom prefers to occupy the interstitial site rather than the Pb site. The room-temperature scanning transmission electron microscopy (STEM) images of the sample with 0.75 at% Cu are shown in the bottom panel of Fig. 1. It is obvious that the sample is composed of homogeneous host matrix and nano-sized precipitate segregating at the triangular grain boundary. According to the EDS characterization, the atomic ratio of Cu to Se of the nanoscale precipitate is close to 2 : 1 (see **Fig. S2** in the ESI†). The structural feature near the precipitate is further examined by STEM imaging (the area indicated by the green rectangle). The spacing of 0.30 nm is in agreement with the (200) interplanar distance of the PbSe matrix. The spacings of 0.67 nm and 0.20 nm correspond to the inter- and intra-layer distances of the monoclinic Cu_2Se, respectively. Thus, it can be concluded that most of Cu in our samples exists in the precipitate as a monoclinic Cu_2Se phase, which resides at the grain boundary (see detailed phase characterization and microstructural analysis in the ESI†). With the rising of temperature, the Cu_2Se precipitates start to decompose and Cu ions continuously enter into the interstitial sites of the PbSe lattice. Finally, a single-phase solid solution is formed when the precipitates are completely depleted at high temperatures. The dissolving of the Cu-rich second phase and the diffusion of Cu are confirmed by the in-situ heating STEM characterization (see **Fig. S3** in the ESI†).

Fig. 2 shows the temperature-dependent electrical transport properties of the $PbCu_xSe$ samples. The negative Seebeck coefficients reveal the n-type conduction in all our samples, indicating that Cu atoms acting as electron donors when entering the interstitial sites of PbSe. As shown in Fig. 2(a), the pristine PbSe possesses the lowest electrical conductivity among all the samples due to its low carrier concentration. Significant increase in the room-temperature electrical conductivity is achieved for the $PbCu_xSe$ sample with $x > 0$, originating from the substantial increase in electron concentration. This indicates that the Cu atom serves as an effective dopant to increase the carrier concentration.

For the samples with lower Cu concentrations (x = 0.00125 and 0.0025), the electrical conductivities show the typical behavior of a degenerate semiconductor. However, for the samples with higher Cu concentrations (x = 0.00375, 0.005, and 0.0075), the temperature dependence of electrical conductivities shows a “quasi” degenerate semiconductor behavior with a visible platform around 550 K. This difference in the temperature dependent electrical transport properties

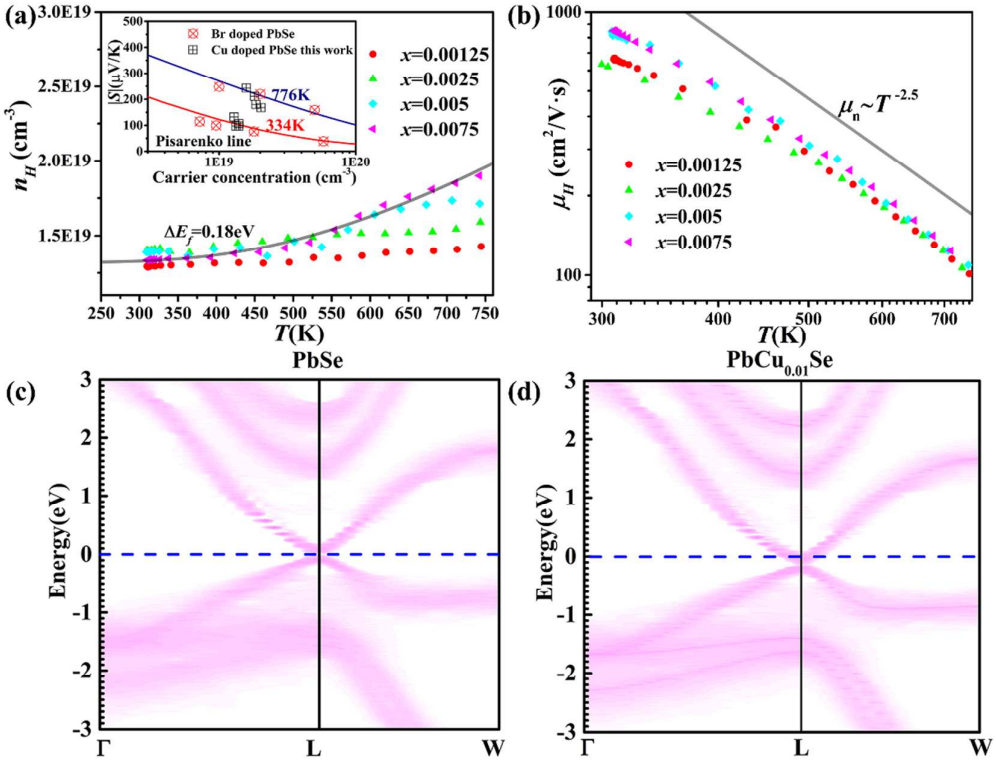

Fig. 3 (a) Temperature dependent charge carrier concentrations of the $PbCu_xSe$ samples. The solid black line is the fitting result for the ascending part of the carrier concentration *vs*. temperature curve of the sample with x = 0.0075, where ΔE_f is the obtained formation energy of an interstitial Cu. The inset of (a) shows the carrier concentration dependence of Seebeck coefficient for the Cu-doped PbSe sample at different temperatures by using single parabolic band model assuming that the acoustic phonon dominates the charge transport. (b) Temperature dependent carrier mobilities of the samples with x = 0.0125, 0.0025, 0.005 and 0.0075. (c) and (d) electronic band structures at 800 K for PbSe and $PbCu_{0.01}Se$, respectively. All the Fermi levels are set to be the zero energy points. Each band structure is obtained by averaging the band structures for 16 snapshots in the *ab initio* molecular dynamics.

can be easily understood based on the schematic phase diagram shown in Fig. 2(b). For the sample with lower Cu content, it is a single-phase solid solution. The Cu atom, acting as a donor, resides in the interstitial site of the PbSe lattice. Therefore, the samples with lower Cu concentrations (x = 0.00125 and 0.0025) shows the typical degenerate semiconductor behavior. With the increase of Cu content, Cu_2Se precipitates present in the sample due to the limited solid solubility of Cu in PbSe at room temperature. With the rising of temperature, Cu_2Se precipitates gradually dissolve into the PbSe matrix and the Cu ions diffuse into the interstitial sites of PbSe matrix because the solid solubility of Cu in PbSe increases with the rising temperature. The intercalation of Cu into the interstitial sites of PbSe provides extra electrons, and so abnormal electrical transport behavior is observed in the temperature dependent electrical conductivity curve for the samples with higher Cu contents (x = 0.00375, 0.005, and 0.0075).

As shown in Fig. 2(c), the trend of temperature dependent Seebeck coefficient is basically consistent with that of temperature dependent electrical conductivity, showing also the degenerate semiconductor behavior. The absolute value of Seebeck coefficient reduces gradually with the increase of Cu content because the electron carrier concentration increases with the Cu atom occupying the interstitial site. Similar to the abnormal behavior shown in the electrical conductivity, the upward bulge shown in the temperature dependent Seebeck coefficient can also be ascribed to the dissolving of the Cu_2Se precipitates.

Benefiting from the dynamic doping effect, the carrier concentrations are optimized over a wide temperature range in our PbSe-Cu system. Therefore, the decline of Seebeck coefficients with the increasing temperature is well compensated, and enhanced power factors ($PF = S^2\sigma$) throughout the measured temperature range are obtained for the $PbCu_xSe$ sample with $x > 0$. As shown in Fig. 2(d), the power factors of the samples with x = 0.0025, 0.00375, 0.005 and 0.0075 reach 16 ~ 21 μW cm^{-1} K^{-2} in the measured temperature range. It should be noted that, for the samples with higher Cu contents, further decrease of the power factor with the increasing temperatures is effectively prevented and visible platforms in the *PF vs*. *T* curves can be observed, which can be ascribed to the increase of the carrier concentration with the rising temperature. Consequently, the Cu-doped PbSe samples possess relatively high power factors in the whole measuring temperature range.

The electrical transport properties of the Cu-containing samples can be better understood by the temperature

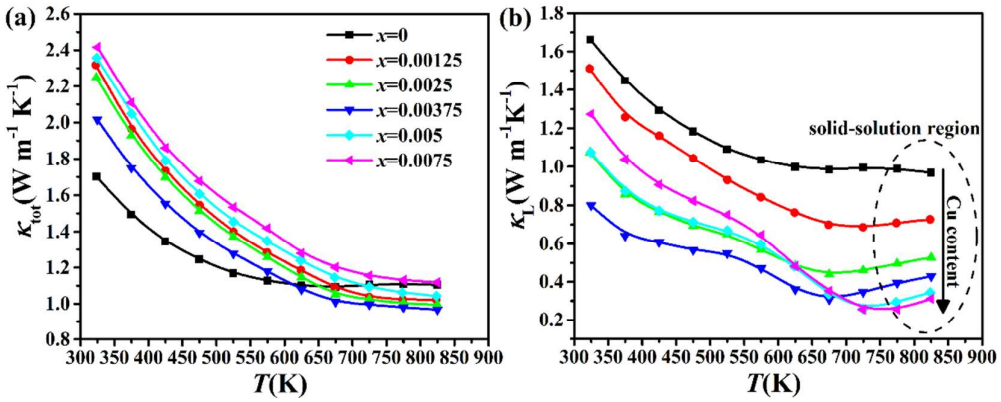

Fig. 4 Temperature dependent (a) total thermal conductivity and (b) lattice thermal conductivity of the $PbCu_xSe$ sample.

dependent carrier concentrations shown in **Fig. 3(a)**. Compared with the samples with lower Cu contents, the carrier concentrations of the samples with higher Cu contents (x = 0.005 and 0.0075) show strongly temperature dependent behavior. Generally, the carrier concentration of a heavily doped semiconductor is a constant and does not change with the temperature. As shown in Fig. 3(a), the carrier concentrations of the samples with lower Cu contents (x = 0.00125 and 0.0025) do not vary significantly with the temperature, indicating these samples are single-phase solid solutions and all the Cu ions are located in the interstitial sites of the PbSe lattice. This is consistent with the temperature dependent electrical conductivity shown in Fig. 2(a). However, for the samples with higher Cu contents (x = 0.005 and 0.0075), their carrier concentrations increase with the increase of temperature, resulting from the dissolving of the Cu-rich second phase into the PbSe matrix. Upon raising of temperature, the Cu-rich second phase continuously dissolves into the PbSe matrix and the Cu ions diffuse into the interstitial sites of the PbSe lattice, and thus the carrier concentration increases with the temperature. It is to note that here the increasing carrier concentration with temperature should not be attribute to the bipolar effects because of the relative high initial carrier concentration (>1×10^{19} cm^{-3}) of our Cu doped samples (see **Fig. S4** and related discussions on the distinction between the proposed dynamic doping effect and bipolar effect in ESI†). The formation energy (ΔE_f), which is the energy required to form a Cu interstitial, is also derived from the ascending part of the temperature dependent carrier concentration curve using the exponential relationship of $e^{\Delta E_f/T}$. For the sample with x = 0.0075, the formation energy is ~0.18 eV and is smaller than those of interstitial Ag[16] and Pb[22] in PbTe system, which means it is easier to produce a Cu interstitial in PbSe.

As has been well established in thermoelectric materials, the Pisarenko line (Seebeck coefficient *vs*. carrier concentration curve) provides a powerful tool to characterize the band structure of a thermoelectric material.[23,24] By using a single parabolic band (SPB) model and assuming the acoustic phonon dominates the charge transport, the Pisarenko lines at 334 and 776 K are plotted (the inset of Fig. 3(a)). The data for Br-doped PbSe from literature[25] are also included for comparison. As shown in the inset of Fig. 3(a), the Seebeck coefficients of our samples almost situate in the Pisarenko lines at both 334 and 776 K, implying that the band structure is not changed by intercalating Cu. It is to note that this is also confirmed by our theoretical calculations. Fig. 3(c) and (d) present the band structures for pristine PbSe and Cu-doped PbSe, respectively. Each band structure is obtained by averaging the band structures for 16 snapshots in the *ab initio* molecular dynamics (AIMD). According to our calculation, the interstitial Cu ions do not alter the conduction band minimum (CBM). Instead, they move the Fermi level upwards into the CBM (Fig. 3(d)). Similarly, the electronic density of states (see **Fig. S5** in the ESI†) show that the electronic states of Cu are far from the CBM. The integration of the DOS from CBM to the Fermi level (zero energy point) indicates that each Cu ion donates one electron. These results demonstrate that IB elements only serve as +1 electron dopants when sitting at the interstitial sites of IV-VI compounds, similar to the case of alkaline metals in $CoSb_3$.[26]

Since the Cu ions occupying the interstitial sites of PbSe have only little influence on the conduction band minimum which dominates the electron transport, the interstitial site might serve as the ideal doping site to regulate the electrical transport properties of n-type PbSe. The temperature dependences of carrier mobilities of the Cu-doped PbSe samples are presented in Fig. 3(b). In general, the Cu-doped samples have much high mobilities in a wide temperature range. The carrier mobilities of these samples decrease rapidly with the increase of temperature, following approximately the relationship $\mu \propto T^{-2.5}$ (especially in the high temperature region). This is a conventional behavior for heavily doped n-type PbSe, suggesting the acoustic phonon dominates the charge carrier scattering.[25,27] Thus, it can be concluded that the introduction and rapid motion of Cu ions do not change the electron scattering mechanism in the PbSe lattice, which might be ascribed to the low concentration and much smaller ionic radius of Cu^+ (0.6 Å). Similar results have also been reported in the Mn-doped SnTe-Cu_2Te[28, 29] and Ag-doped PbTe-Ag_2Te systems.[16] Both Ag in PbTe [16] and Cu in PbSe serve

as n-type dopants. We have calculated the formation energies of the following reactions,

$$0.0093Cu+PbSe \rightarrow Cu_{0.0093}PbSe \quad , \quad \Delta H_1$$

$$0.0093Ag+PbTe \rightarrow Ag_{0.0093}PbTe \quad . \quad \Delta H_2$$

Our results show that ΔH_1=0.0115 eV, which is 0.0037 eV lower than ΔH_2. The calculation is consistent with the formation energy difference (0.18 eV vs. 0.23 eV[16]) and initial carrier density (1×10^{18} cm^{-3} [16] for Ag doped PbTe-Ag_2Te systems *vs* 1×10^{19} cm^{-3} for our PbSe-Cu_2Se systems) of the two doping systems. Our theoretical and experimental results imply that the Cu is a better candidate for the dynamic doping element than Ag.

at high temperatures, indicating that the lattice thermal conductivities of the Cu-doped samples are effectively reduced. According to a recent work,[28] the interstitial Cu is very effective on reducing the lattice thermal conductivity. Fig. 4(b) shows the lattice thermal conductivities of all the samples calculated by subtracting κ_e from κ_{tot}. According to the Wiedmann-Franz law, $\kappa_e = L\sigma T$, where L is the Lorentz number (see the ESI† for the detailed calculation of L). Surprisingly, it can be observed in Fig. 4(b) that the κ_L *vs*. T curves for Cu-containing samples exhibit a valley-like shape, and the sample with higher Cu content has a sharper and deeper valley. Furthermore, assuming that the phonon U-

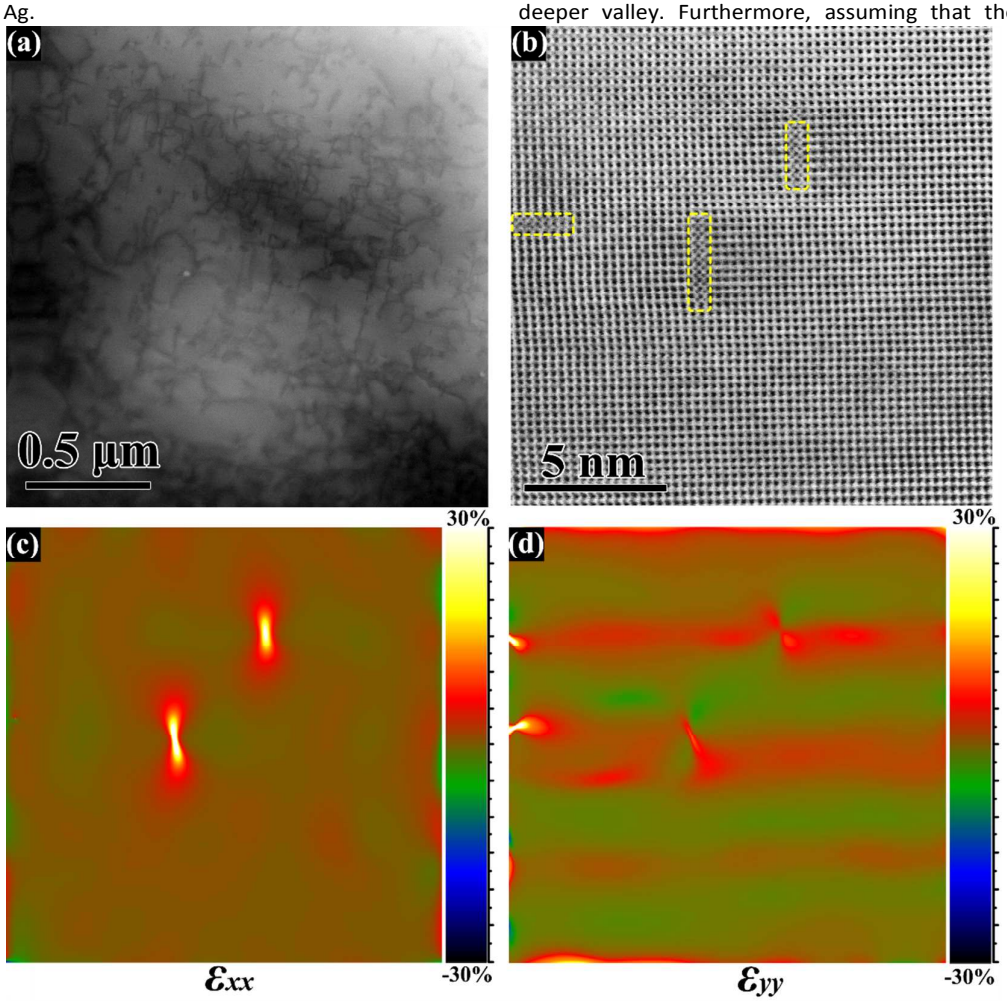

Fig. 5 (a) low-magnification STEM image of uniformly distributed dense dislocations and (b) ABF STEM image of some perpendicular and parallel platelet-like precipitates in the $PbCu_{0.0075}Se$ sample. Parts (c) and (d) are the GPA strain maps derived from (b) along x (ε_{xx}) and y (ε_{yy}) directions.

The interstitial Cu ions in the rigid lattice of PbSe also give rise to an intriguing phenomenon in the thermal conductivity. As shown in **Fig. 4(a)**, the Cu-containing samples exhibit higher total thermal conductivities at low temperatures than the pure PbSe sample, which can be ascribed to the increased electronic thermal conductivities due to the doping of Cu (see **Fig. S6** in the ESI†). However, the total thermal conductivities of the Cu-doped samples are smaller than that of the pure PbSe sample

process is the dominant scattering mechanism, the lattice thermal conductivity will follow the T^{-1} relationship.[30] It is obviously that the lattice thermal conductivity of the Cu-doped sample deviates significantly from the typical T^{-1} relationship at high temperatures.

The abnormal thermal transport properties of the Cu-doped PbSe samples can be ascribed to their complexity in microstructures. Thus, the crystal imperfections closely

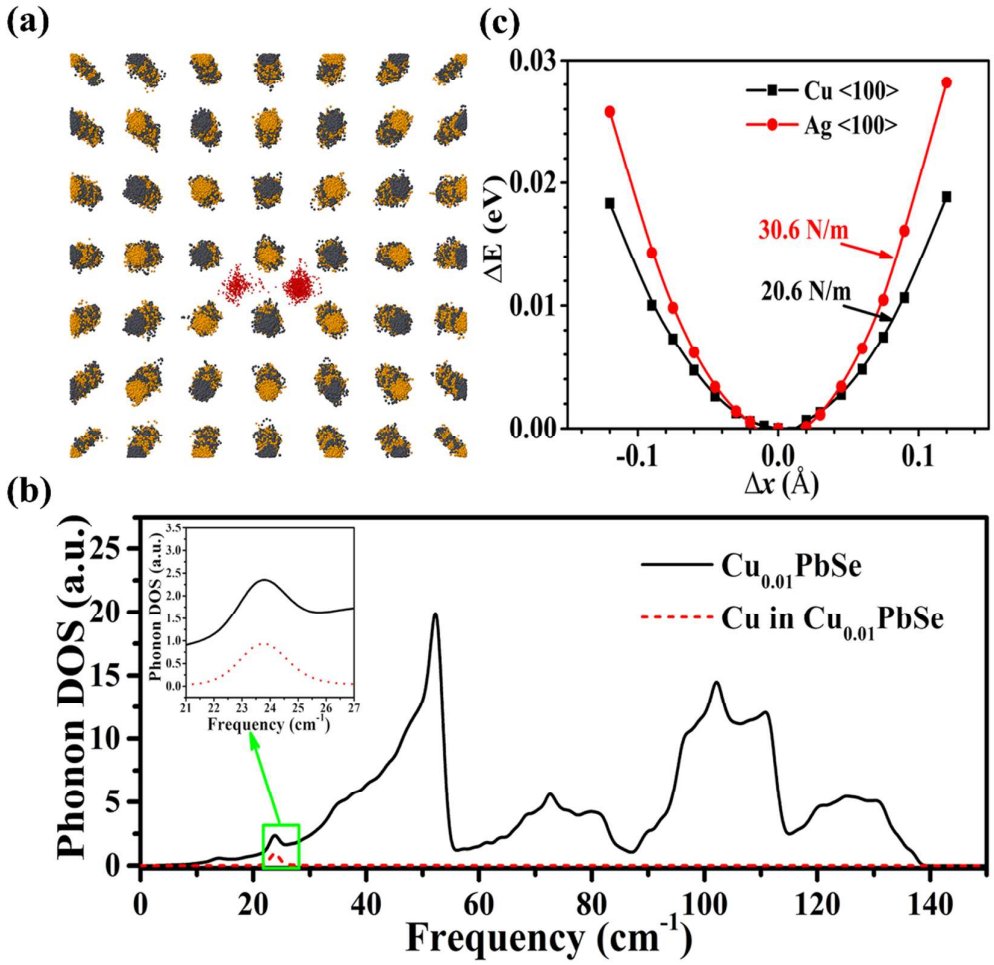

Fig. 6 (a) The *ab initio* molecular dynamics trajectory of all the atoms in $PbCu_{0.01}Se$ at 800 K. (b) Total phonon density of states of $PbCu_{0.01}Se$ at 800K and partial contribution from Cu. (c) The potential wells of Cu and Ag vibrating around the interstitial sites of PbSe.

correlated with the multi-scale phonon scattering in the Cu-doped PbSe samples haven been investigated by STEM, annular bright-field (ABF) STEM, and high-angle annular dark-field (HAADF) STEM techniques. It can be found that the intercalation of Cu ions leads to a high density of uniformly distributed dislocations at room temperature (**Fig. 5(a), Fig. S7, Fig. S8(a)** and related discussions in the ESI†). Meanwhile, Cu_2Se precipitates at the grain boundaries (Fig. 1) and platelet-like nanoclusters in the size of several nanometers are also observed in the PbSe matrix at room temperature (see the ABF and corresponding HAADF STEM images in Fig. 5(b) and Fig. S8(b) in the ESI†, respectively). It seems that the nanoscale clusters shown in Fig. 5(b) are formed from the ordered aggregation of interstitial atoms, which may relate to the non-equilibrium intercalation of Cu ions. Thus, it is conceivable that the intercalated Cu ions may also lead to prominent lattice distortions. Strain maps derived from Fig. 5(b) by geometric phase analysis (GPA)[31] are presented in Fig. 5(c) (ε_{xx}) and 5(d) (ε_{yy}), which clearly show the strains along the *x* and *y* directions, respectively. It can be inferred from Fig. 5(c) and 5(d) that the strains induced by the platelet-like nanoclusters exhibit an anisotropic behavior, which mainly distribute along the direction perpendicular to the platelets. The hierarchical architectures in the $PbCu_xSe$ sample, including nano-precipitates, nano-clusters, strains and dislocations, as well as the on-site vibration of Cu ions around the interstitial sites (see below), result in enhanced phonon scattering and significantly decreased lattice thermal conductivities around room temperature, as shown in Fig. 4(b). With the increasing temperature, the interstitial Cu atoms increase because of the increased solid solubility of Cu in the PbSe lattice, which shall lead to reduced lattice thermal conductivity. However, the number of dislocations and nanoscale clusters as well as the intensity of strains decrease gradually, and the Cu_2Se nano-precipitates continuously dissolve into the PbSe matrix with the rising of temperature, which shall result in increased lattice thermal conductivity. As a result, the complexity of the microstructure itself and its complicate evolution with the temperature contribute to the deviation of T^{-1} law as well as the valley-like feature of κ_L *vs.* *T* curves of the Cu-doped PbSe samples due to the competition between different phonon scattering centres. We also believe that some other factors

might also affect the lattice thermal conductivity due to the complexity of the Cu-doped PbSe system. For example, the diffusion process of the Cu ions may give rise to additional phonon scattering, and the specific heat might also have a small effect from the intercalation reaction with Cu at higher temperatures (In this work, we use the same C_p as use previously for direct comparison with the prior works). The sudden drop in κ_L can also be found in previous literatures despite that the reason has not been given. For example, a sharp drop in κ_L is observed in the Na-doped PbTe system,[32-34] and we propose that the drop in κ_L is associated with the dissolving of the Na dopant.

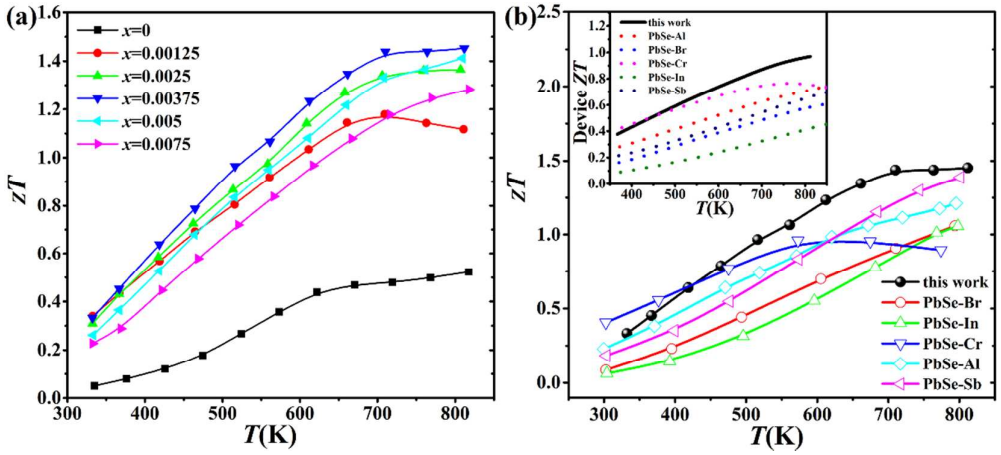

Fig. 7 (a) Figure of merit zT of the $PbCu_xSe$ samples. (b) Comparison of zT and device ZT of n-type PbSe in this work with those in previous reports.[25,27,38-40]

In addition, it can be found in the solid solution region shown in Fig. 4(b) that the lattice thermal conductivity decreases continuously with the increasing Cu content. In order to understand the role of Cu in reducing the lattice thermal conductivity at high temperatures, AIMD study has been performed for the $PbCu_{0.01}Se$. The temperature of the AIMD is 800 K, which is consistent with the high temperature nature of the solid solution region. From the AIMD trajectory (**Fig. 6(a)**), a distinct feature is that at high temperatures, Cu ions in PbSe vibrate around the interstitial sites, and the displacements are comparable with those of Pb and Se atoms. These vibrations of Cu atoms result in low-lying optical phonons at around 23-25 cm^{-1}, as shown in Fig. 6(b). The frequency range of these phonons is comparable with those of other compounds with low lattice thermal conductivities (for example, 16 cm^{-1} for Ag in MgAgSb[19], 42 cm^{-1} for Yb in Yb_xCoSb_3[35]). These optical phonons provide enhanced phonon scattering channels,[35] which will become one of the fundamental reasons for the lowered lattice thermal conductivities in the solid solution stage at high temperatures. In addition to the vibrating motions, Cu atoms can even hop between interstitial sites, which may lead to additional phonon scatterings as those compounds, eg. Cu_2Se and Cu_2Te, with fast moving ions.[36]

The reason for the low frequency of the optic phonons caused by Cu atoms can be rationalized by the low force constants. Fig. 6(c) shows the potential wells of Cu and Ag atoms at the interstitial sites of PbSe, moving along [100] direction. The potential well of Cu is below that of Ag, resulting in a lower force constant as of 20.6 N/m (30.6 N/m for Ag). This force constant of Cu in PbSe is even lower than most of the fillers vibrating in the much larger crystalline voids of $CoSb_3$.[35] The origin of the low force constant is from 1) the monovalent charge state of Cu; and 2) the small atomic size. Hence, for the thermal transport of Cu-doped PbSe, the complexity of its microstructure and vibration of Cu ions at higher temperature provide phonon scattering centers in various scales, leading to reduced lattice thermal conductivities in a wide temperature range.

By virtue of the extraordinary electrical and thermal transport properties of our PbSe-Cu system in a wide temperature range, remarkably enhanced zT values are obtained. The maximum zT for the sample with x = 0.00375 is up to 1.45 at 813 K, which precedes most of the n-type PbSe-based materials (see **Fig. 7(a)** and 7(b)). To evaluate its potential for practical application, the thermoelectric device figure of merit ZT has been calculated (see the recent work for the detailed calculation of device ZT).[37] As shown in the inset of Fig. 7(b), the device ZT (for a thermoelectric generator) of the $PbCu_xSe$ sample with x = 0.00375 is superior to the

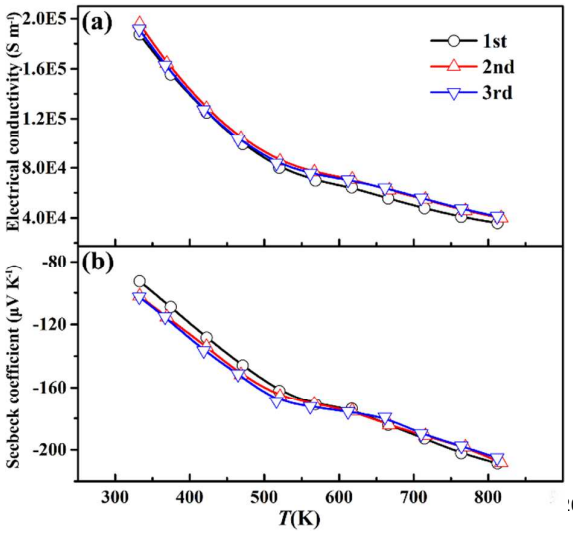

Fig. 8 Temperature dependent (a) electrical conductivity and (b) Seebeck coefficient of the $PbCu_xSe$ sample with x = 0.00375 measured in the first, second and third heating process.

previously reported n-type PbSe-based materials,[25,27,38-40] which can be ascribed to the optimized carrier concentration due to the continuous carrier injection with the rising of temperature as well as the ultra-low lattice thermal conductivity in a wide temperatures range resulted from the hierarchical phonon scattering (detailed discussions on the comparison of the electrical and thermal transport properties for PbSe with dynamic Cu doping and the conventional doping can be found in section 6 of the ESI† and **Fig. S9**, **Fig. S10**, and **Fig. S11**). It is worth noting that the Cu intercalated PbS system shows similar thermoelectric transport properties to PbSe-Cu_2Se systems (see **Fig. S12** in the ESI†), demonstrating that the intercalation of Cu ions could be used as a universal and effective strategy to optimize the thermoelectric performance of other materials.

Thermal stability is also a priority issue for the practical application of thermoelectric materials.[41] As for our PbSe-Cu system, the superior device *ZT* is mainly contributed by the optimized carrier concentration over the whole measured temperature range. Thus, the electrical transport properties of the samples have been repeatedly measured for three times. **Fig. 8(a)** and 8(b) show the electrical conductivity and Seebeck coefficient, respectively, for the $PbCu_xSe$ sample with x = 0.00375 measured in the first, second and third heating process. As shown in Fig. 8, all the electrical transport data exhibit good reproducibility. In order to further evaluate the long-term service performance of our PbSe-Cu system, all the thermoelectric properties have also been repeatedly measured for three heating-cooling cycles (see Fig. **S13~S15** in the ESI†). It can be derived from the cycling measurements that the achieved highest *zT* and device *ZT* for all the samples are highly preserved after several repeated heating-cooling processes. In addition, according to our SEM characterization (**Fig. S16**), the composition of the repeatedly measured sample is uniform, and no aggregated Cu-related impurities can be detected at the end contacting the hot source or cold sink. This means that the Cu atoms do not migrate along the temperature gradient applied during the measurement. Therefore, the thermal stability of the constructed PbSe-Cu system is superior to other thermoelectric materials involving dissolution, diffusion, or fast motion of ions.[4-6]

Conclusions

In summary, the unique effects of Cu intercalation on both the electrical and thermal transport properties are first disclosed in bulk PbSe system. Based on the fast diffusion of Cu ions into the interstitial sites of PbSe, the electron concentration of the system can be optimized in a wide temperature range, which is superior to other conventional n-type doping methods. Furthermore, unexpected low thermal conductivities for the $PbCu_xSe$ system are also demonstrated because of hierarchical phonon scattering. Consequently, both the peak *zT* and the device *ZT* of the n-type PbSe system are substantially boosted. The maximum material *zT* and device *ZT* of the sample with x = 0.00375 reach ~1.45 and unity at 813 K, respectively. Moreover, the introduction of interstitial Cu ions and their fast motion have negligible effect on the dispersion of the conduction band, ensuring that the intercalation of Cu is an independent method to safely modulate the carrier concentration of the n-type PbSe system. Thus, this can be used as a fundamental optimization route prior to the others, such as band engineering. The intercalation of Cu might be a generally applicable route to improve the thermoelectric performance since the dynamic behaviors of Cu ions could present in other IV-VI compounds.

Experimental

Sample synthesis:

High purity Pb shots (99.999%, Aladdin, China), Te chunks (99.999%, Aladdin, China), and Cu pieces (99.999%, Sigma-Aldrich, USA) were used as the starting materials to synthesize $PbCu_xSe$ (x = 0, 0.00125, 0.0025, 0.00375, 0.005 and 0.0075). The raw materials were weighed and loaded into silica tubes under an Ar-filled glove box, and then flame-sealed under vacuum. The silica tubes were heated up to 1383 K in 10 h, soaked at this temperature for 10 h and subsequently cooled to room temperature in the furnace. The obtained ingot was ground into fine powders and then compacted in a graphite die by vacuum hot pressing with a pressure of 65 MPa at the temperature of 873 K for 20 min, yielding samples with over 98% of the theoretical density.

Phase identification and thermoelectric properties measurement:

Phase identification was carried out by X-ray powder diffraction (XRD) using a Rigaku D/max-2200 diffractometer with Cu Kα radiation at room temperature. The hot-pressed discs were cut into the bars with the size about 2 mm × 3 mm × 15 mm for Seebeck coefficient and resistivity measurements conducted on a ZEM-3 system (ULVAC-RIKO, Japan) under the protection of helium gas. The thermal diffusivities (α) of the samples were measured by a Netzsch LFA 457 laser flash apparatus with the Cowan model plus pulse correction. The thermal conductivity was calculated via $\kappa = C_p \times D \times \alpha$, where κ is the total thermal conductivity, C_p the heat capacity, D the actual density of the sample, and α the thermal diffusivity. The sample density (D) was determined by the Archimedes method, and the heat capacity (C_p) was estimated from the typical calculation for lead chalcogenides, C_p (k_B/atom) = 3.07 + 0.00047 × (T - 300). Temperature dependent carrier concentrations and mobilities of the samples were obtained from Hall coefficient measurements using a four-probe Van der Pauw technique under a reversible magnetic field of 1.5 T. The details on the estimation of Hall factor can be found elsewhere.[42]

Microstructure analysis:

The microstructure of PbSe-Cu sample was characterized by spherical aberration-corrected scanning transmission electron microscopy (STEM) using a JEM-ARM 200F transmission electron microscope (TEM). Bright field and high-angle annular

dark field (HAADF) imaging was performed in the STEM mode on samples after the measurements of thermoelectric properties. STEM specimens were prepared by mechanical slicing, polishing, and dimpling, followed by ion-milling with liquid nitrogen. Energy-dispersive X-ray spectroscopy (EDS) was used to determine the sample composition on a Zeiss GeminiSEM 300 scanning electron microscope equipped with an EDXS detector (Oxford Instrument). *In-situ* STEM and electron energy loss spectroscopy (EELS) elemental mapping were conducted on a FEI Titan Themis spherical aberration corrected STEM.

Theoretical methods:

All the first principles calculations in this study were performed by using Vienna *ab initio* simulation package (VASP).[43] Generalized gradient approximation of the form Perdew–Burke–Ernzerhof [44] and projected augmented wave methods[45,46] were adopted in the calculations. Ab initio molecular dynamics (AIMD) simulation was also performed in the VASP code with the canonical ensemble. The chemical formula in the AIMD study was $Pb_{108}Cu_1Se_{108}$. The simulation time was longer than 60 ps (with a time step of 2 fs) to ensure the convergence. And the Temperature Dependent Effective Potential (TDEP) method developed by Hellman et al.[47,48] was applied for extracting the temperature dependent interatomic force constants (IFCs) and subsequent phonon density of states.

Conflicts of interest

There are no conflicts to declare.

Acknowledgements

This work was supported by the National Natural Science Foundation of China (Grant No. 51371194, 51772186, 51572167, 51632005, and 11674211), National Key Research and Development Program of China (No. 2017YFB0701600), the 111 Project D16002, and the research grant (No. 16DZ2260601) from Science and Technology Commission of Shanghai Municipality. JY acknowledges support from the Program for Professor of Special Appointment (Eastern Scholar) at Shanghai Institutions of Higher Learning (No. TP2015041) and Natural Science Foundation of Shanghai (No. 16ZR1448000). W.Z. acknowledges the support from the Program of Shanghai Subject Chief Scientist (No. 16XD1401100). G.J.S. acknowledges S^3TEC - EFRC funded by the U.S. Department of Energy, award number DE-SC0001299. We thank Prof. J. Q. He and Dr. L. Xie for the in-situ STEM characterization. J.L thanks the fruitful discussion with Prof. J. H. Yang at University of Washington.

Notes and references

1 H. Liu, X. Shi, F. Xu, L. Zhang, W. Zhang, L. Chen, Q. Li, C. Uher, T. Day, G. J. Snyder, *Nat. Mater.* 2012, **11**, 422.
2 R. Nunna, P. Qiu, M. Yin, H. Chen, R. Hanus, Q. Song, T. Zhang, M.-Y. Chou, M. T. Agne, J. He, G. J. Snyder, X. Shi, L. Chen, *Energy Environ. Sci.* 2017, **10**, 1928.
3 S. Lee, K. Hippalgaonkar, F. Yang, J. W. Hong, C. Ko, J. Suh, K. Liu, K. Wang, J. J. Urban, X. Zhang, C. Dames, S. A. Hartnoll, O. Delaire, J. Q. Wu, *Science* 2017, **355**, 371.
4 A. Bohra, R. Bhatt, S. Bhattacharya, R. Basu, S. Ahmad, A. Singh, D. K. Aswal, S. K. Gupta, *AIP Conf. Proc.* 2016, **1731**, 110010.
5 H. Zhu, J. Luo, H. Zhao, J. Liang, *J. Mater. Chem. A* 2015, **3**, 10303.
6 A. A. Olvera, N. A. Moroz, P. Sahoo, P. Ren, T. P. Bailey, A. A. Page, C. Uher, P. F. P. Poudeu, *Energy Environ. Sci.* 2017, **10**, 1668.
7 L. E. Bell, *Science* 2008, **321**, 1457.
8 T. Zhu, Y. Liu, C. Fu, J. P. Heremans, J. G. Snyder, X. Zhao, *Adv. Mater.* 2017, **29**, 1605884.
9 G. Tan, L. D. Zhao, M. G. Kanatzidis, *Chem. Rev.* 2016, **116**, 12123.
10 J. Yang, L. Xi, W. Qiu, L. Wu, X. Shi, L. Chen, J. Yang, W. Zhang, C. Uher, D. J. Singh, *npj Computational Materials* 2016, **2**, 15015.
11 A. F. Ioffe, *Semiconductor thermoelements, and Thermoelectric cooling*, Infosearch, London, 1957.
12 Y. Pei, Z. M. Gibbs, A. Gloskovskii, B. Balke, W. G. Zeier, G. J. Snyder, *Adv. Energy Mater.* 2014, **4**, 1400486.
13 Y. Z. Pei, A. D. LaLonde, N. A. Heinz, X. Y. Shi, S. Iwanaga, H. Wang, L. D. Chen, G. J. Snyder, *Adv. Mater.* 2011, **23**, 5674.
14 Z. Dashevsky, S. Shusterman, M. P. Dariel, I. Drabkin, *J. Appl. Phys.* 2002, **92**, 1425.
15 V. L. Kuznetsov, L. A. Kuznetsova, A. E. Kaliazin, D. M. Rowe, *J. Mater. Sci.* 2002, **37**, 2893.
16 Y. Pei, A. F. May, G. J. Snyder, *Adv. Energy Mater.* 2011, **1**, 291.
17 F. F. Kharakhorin, D. A. Gambarova, V. V. Aksenov, *Sov. Phys. -Sol. State* 1966, **7**, 2813.
18 Y. He, T. Day, T. S. Zhang, H. L. Liu, X. Shi, L. D. Chen, G. J. Snyder, *Adv. Mater.* 2014, **26**, 3974.
19 P. Ying, X. Li, Y. Wang, J. Yang, C. Fu, W. Zhang, X. Zhao, T. Zhu, *Adv. Funct. Mater.* 2017, **27**, 1604145.
20 C. Gayner, R. Sharma, I. Mallik, M. K. Das, K. K. Kar, *J. Phys. D Appl. Phys.* 2016, **49**, 285104.
21 C. Schneider, P. Schichtel, B. Mogwitz, M. Rohnke, J. Janek, *Solid State Ionics* 2017, **303**, 119.
22 E. Miller, K. Komarek, I. Cadoff, *J. Appl. Phys.* 1961, **32**, 2457.
23 L. Wu, X. Li, S. Wang, T. Zhang, J. Yang, W. Zhang, L. Chen, J. Yang, *NPG Asia Mater.* 2017, **9**, e343.
24 L. D. Zhao, G. J. Tan, S. Q. Hao, J. Q. He, Y. L. Pei, H. Chi, H. Wang, S. K. Gong, H. B. Xu, V. P. Dravid, C. Uher, G. J. Snyder, C. Wolverton, M. G. Kanatzidis, *Science* 2016, **351**, 141.
25 H. Wang, Y. Pei, A. D. LaLonde, G. J. Snyder, *Proc. Natl. Acad. Sci. USA* 2012, **109**, 9705.
26 S. Y. Wang, J. R. Salvador, J. Yang, P. Wei, B. Duan, J. H. Yang, *NPG Asia Mater.* 2016, **8**, e285.
27 Y. Lee, S. H. Lo, C. Chen, H. Sun, D. Y. Chung, T. C. Chasapis, C. Uher, V. P. Dravid, M. G. Kanatzidis, *Nat. Commun.* 2014, **5**, 3640.
28 Y. Pei, L. Zheng, W. Li, S. Lin, Z. Chen, Y. Wang, X. Xu, H. Yu, Y. Chen, B. Ge, *Adv. Electron. Mater.*2016, **2**, 1600019.
29 W. Li, L. Zheng, B. Ge, S. Lin, X. Zhang, Z. Chen, Y. Chang, Y. Pei, *Adv. Mater.* 2017, **29**, 1605887.
30 J. Luo, L. You, J. Zhang, K. Guo, H. Zhu, L. Gu, Z. Yang, X. Li, J. Yang, W. Zhang, *ACS Appl. Mater. Interfaces* 2017, **9**, 8729.
31 M. J. Hytch, E. Snoeck, R. Kilaas, *Ultramicroscopy* 1998, **74**, 131.
32 K. Biswas, J. He, I. D. Blum, C. I. Wu, T. P. Hogan, D. N. Seidman, V. P. Dravid, M. G. Kanatzidis, *Nature* 2012, **489**, 414.

33 Z. Chen, Z. Jian, W. Li, Y. Chang, B. Ge, R. Hanus, J. Yang, Y. Chen, M. Huang, G. J. Snyder, Y. Pei, *Adv. Mater.* 2017, **29**, 1606768.
34 S. N. Girard, J. He, X. Zhou, D. Shoemaker, C. M. Jaworski, C. Uher, V. P. Dravid, J. P. Heremans, M. G. Kanatzidis, *J. Am. Chem. Soc.* 2011, **133**, 16588.
35 J. Yang, W. Zhang, S. Q. Bai, Z. Mei, L. D. Chen, *Appl. Phys. Lett.* 2007, **90**, 192111.
36 S. Ballikaya, H. Chi, J. R. Salvador, C. Uher, *J. Mater. Chem. A* 2013, **1**, 12478.
37 G. J. Snyder, A. H. Snyder, *Energy Environ. Sci.* 2017, **10**, 2280.
38 [38] Q. Zhang, H. Wang, W. Liu, H. Wang, B. Yu, Q. Zhang, Z. Tian, G. Ni, S. Lee, K. Esfarjani, G. Chen, Z. Ren, *Energy Environ. Sci.* 2012, **5**, 5246.
39 Q. Zhang, E. K. Chere, K. McEnaney, M. L. Yao, F. Cao, Y. Z. Ni, S. Chen, C. Opeil, G. Chen, Z. F. Ren, *Adv. Energy Mater.* 2015, **5**, 8.
40 Q. Zhang, F. Cao, K. Lukas, W. Liu, K. Esfarjani, C. Opeil, D. Broido, D. Parker, D. J. Singh, G. Chen, Z. Ren, *J. Am. Chem. Soc.* 2012, **134**, 17731.
41 D. M. Rowe, *Thermoelectrics handbook : macro to nano*, CRC/Taylor & Francis, Boca Raton 2006.
42 Y. Pei, A. D. LaLonde, H. Wang, G. J. Snyder, *Energy Environ. Sci.* 2012, **5**, 7963.
43 G. Kresse, J. Furthmuller, *Phys. Rev. B* 1996, **54**, 11169.
44 J. P. Perdew, K. Burke, M. Ernzerhof, *Phys. Rev. Lett.* 1996, **77**, 3865.
45 G. Kresse, D. Joubert, *Phys. Rev. B* 1999, **59**, 1758.
46 P. E. Blöchl, *Phys. Rev. B* 1994, **50**, 17953.
47 O. Hellman, I. A. Abrikosov, *Phys. Rev. B* 2013, **88**, 144301.
48 O. Hellman, P. Steneteg, I. A. Abrikosov, S. I. Simak, *Phys. Rev. B* 2013, **87**, 104111.

Cu intercalation is demonstrated to enhance the thermoelectric performances of PbSe by the dynamic doping effect and hierarchical phonon scattering.